Journal of Colloid and Interface Science 348 (2010) 649–653

Contents lists available at ScienceDirect

Journal of Colloid and Interface Science

www.elsevier.com/locate/jcis

Novel electroless copper deposition on carbon fibers with environmentally friendly processes

Jeong Hoon Byeon [a], Jang-Woo Kim [b,*]

[a] LCD Division, Samsung Electronics Co., Ltd., Yongin 446-711, Republic of Korea
[b] Department of Digital Display Engineering, Hoseo University, Asan 336-795, Republic of Korea

ARTICLE INFO

Article history:
Received 5 March 2010
Accepted 2 May 2010
Available online 7 May 2010

Keywords:
Electroless copper deposition
Carbon fiber (CF)
Environmentally friendly process
Silver (Ag) aerosol activation
Nonformaldehyde ELD

ABSTRACT

A novel electroless deposition (ELD) of copper (Cu) on carbon fibers (CFs) with environmentally friendly processes, silver (Ag) aerosol activation and subsequent nonformaldehyde Cu ELD, was developed. Spark-generated Ag aerosol nanoparticles (~10 nm in mode diameter) were deposited (48.4 μg Ag/g CF in activation intensity) onto the surfaces of CFs. After annealing (at 220 °C in a nitrogen atmosphere), the catalytically activated CFs were placed into a solution for Cu ELD (at 82 °C). Homogeneous Cu coating (~5.1 nm/min) on CFs was achieved with 90 min of deposition and the corresponding mass deposition rate and Cu grain size for 30–90 min of deposition had ranges of 0.25–1.14 mg Cu/g CF-min and 14.8–37.2 nm, respectively. The porosity of CFs decreased by depositing the Cu for 30–90 min, and the specific surface area and pore volume of CFs decreased from 1536 to 1399 m^2/g and from 0.65 to 0.57 cm^3/g, respectively.

1. Introduction

Fine metal particle layers or films have a prominent role in modern technology due to their novel physicochemical properties differing significantly from bulk metal phases and have attracted great interest because of their significant potential applications in the field of material sciences [1–4]. Recently, metal layers supported by fibrous materials have been widely exploited for use in the catalytic elimination of environmental pollutants and as membranes for energy-related processes, conductive or optical components for electronic devices, insulators for electromagnetic wave interference, reinforcements, templates, and antimicrobial agents [5–15].

The methods for preparing metal particle layers on fibrous substrates include chemical vapor deposition, electrodeposition, electroless deposition (ELD), etc. The ELD technique enables metallic components such as copper (Cu) to easily and uniformly deposit on surfaces with complex configuration [16] and likewise on fibrous materials [17], without an external electric current, via oxidation–reduction reactions [18]. Initiation of the ELD process is preceded by surface activation to provide the catalytic sites (usually palladium (Pd)) on the material surface [19,20]. Pd particles act as initiators of the following ELD, which were generally derived by tin (Sn) sensitization in conventional activations. However, Sn is not an active catalyst for ELD and thus growth of the Cu deposit was inhibited [21]. Moreover, conventional activations require a long process time and intermittent water rinsing and drying, involve the loss of expensive metal ions, and create environmental pollution problems [22,23]. Some studies have examined methods of advanced activation using lasers [24], ultraviolet (UV) lasers or UV/VUV (vacuum ultraviolet) excimer lamps [25], plasma [26], and ion beams [27]. Recently, Byeon et al. [28] reported catalytic activation of microporous carbon fibers (CFs) via Pd aerosol nanoparticles for use in silver (Ag) coating. However, the above techniques require specialized conditions and/or expensive Pd compounds for coating catalysts [25,29]. In order to circumvent these problems, some studies [19,21,30–32] tried to successfully replace the costlier Pd catalyst with a cheaper Ag catalyst without affecting the properties of Cu coating. Even though a cheaper activation could be performed, it was still necessary to perform wet chemical steps which might also create environmental pollution problems.

In this study, an ELD of Cu on microporous CFs (as support) with environmentally friendly processes was developed. Ag aerosol activation is a simple, inexpensive, and environmentally friendly process and was used to catalytically Ag activate the CFs and thus, to introduce metallic Ag sites onto the CFs surface for nonformaldehyde (glyoxylic acid used) ELD of Cu. Cu ELD solutions have typically contained Cu ions, complexing and reducing agents. Formaldehyde is an effective reducing agent, which is widely used in Cu ELD processes; however, it is banned in many places, and there is a dire need to find alternative reducing agents [33]. Therefore, Cu ELD solutions using nonformaldehyde reducing agents are attractive because of their better environmental safety than ELD using formaldehyde [33–35]. Microporous CFs are widely used in various separation, purification, and catalytic processes [36,37]. Recently, CFs have been used in electric-double-layer capacitor (EDLC) electrodes on account

* Corresponding author. Fax: +82 41 540 5925.
E-mail address: jwkim@hoseo.edu (J.-W. Kim).

0021-9797/$ - see front matter © 2010 Elsevier Inc. All rights reserved.
doi:10.1016/j.jcis.2010.05.008

of their large specific surface area and high electrical conductivity [38]. This work presented an effective strategy to fabricate metal-coated fiber structures because of its process simplicity and environmental friendliness and will provide a conceptual leap for applications of environmental remediation devices, electromagnetic interference shielding materials, energy generation devices, (opto)electronic devices, etc.

2. Materials and methods

Our catalytic surface activation (Fig. 1) involved the spark generation of Ag aerosol nanoparticles and their filtration by rayon-based microporous CFs (38 mm in diameter and 2.6 mm in thickness, KF-1600, Toyobo). A spark was generated between two identical Ag rods (diameter, 3 mm; length, 100 mm, Nilaco, Japan) inside a reactor in a pure nitrogen environment at standard temperature and pressure (STP) [39]. The flow rate of the nitrogen gas, which was controlled by a mass flow controller, was set to 6 L/min. The electrical circuit specifications were as follows: resistance of 0.5 MΩ; capacitance of 10 nF; loading current of 2.2 mA; applied voltage of 2.9 kV; and frequency of 700 Hz. In order to prevent the detachment of nanoparticles from the surface of the CFs, the CFs were separated from the holder and annealed in nitrogen (N_2) gas at 220 °C for 10 min after separating it from the holder. Once the CFs were activated by the aerosol surface activation, the CFs were immersed (Fig. 1) in an ELD solution (80 mL) for the deposition of Cu onto the surface of the activated CFs. The composition of the Cu ELD solution used in the experiment was as follows: $CuSO_4{\cdot}5H_2O$ (3.8 g/L), as the source of Cu ions, ethylenediamine tetraacetic acid (EDTA, 40 g/L), as the complexing agent, glyoxylic acid monohydrate (6.0 g/L), as a reducing agent, and additional agents such as 2,2′-dipyridine polyethylene glycol and RE-610. The pH of the solution was adjusted to approximately 12 with tetramethylammonium hydroxide (TMAH). The bath temperature was maintained at 82 °C. The electrons were transferred across the Ag island and used for the decomposition of Cu ions into Cu atoms, generating Cu layers onto the Ag seeds as a product. The CFs were vigorously rinsed with deionized (DI) water after the ELD to remove the residual and then set aside to be dried.

The size distribution of the Ag aerosol nanoparticles was measured using a scanning mobility particle sizer (SMPS) consisting of an electrostatic classifier (TSI 3085, US), ultrafine condensation particle counter (TSI 3025, US), and aerosol charge neutralizer (NRD 2U500, US). The SMPS system, which measures the mobility equivalent diameter, was operated at a sample flow of 0.3 L/min, a sheath flow of 3 L/min, and a scan time of 180 s (measurement range: 4.61–157 nm). The overall number, area, and mass concentration of the particles were also measured using the SMPS system both upstream and downstream from the CFs. The morphology and microstructure of the spark-generated Ag nanoparticles were analyzed by high-resolution transmission electron microscopy (HRTEM, JEM-3010, Japan) operated at 300 kV. X-ray photoelectron spectroscopy (XPS) measurements of the activated CFs were performed using a Kratos Axis HIS spectrometer with a monochromatized Al Kα X-ray source (1486.6 eV photons). All binding energies (BEs) were referenced to the C1s hydrocarbon peak at 284.6 eV. Field-emission scanning electron microscope (FESEM, JSM-6500F, JEOL, Japan) images and energy dispersive X-ray (EDX, JED-2300, JEOL, Japan) profiles were obtained at an accelerating voltage of 15 kV. The amount of deposited Cu on the CFs was determined by inductively coupled plasma atomic emission spectroscopy (ICPAES, Elan 6000, Perkin–Elmer, USA). X-ray diffraction (XRD) studies of the Cu-deposited CFs were carried out on a Rigaku RINT-2100 diffractometer equipped with a thin-film attachment using Cu Kα radiation (40 kV, 40 mA). The 2θ angles ranged from 10° to 90° at 4°/min by step scanning at an interval of 0.08°. A linear sweep voltammetry (LSV) measurement was carried out using a potentiostat (VERSASTAT3-200, Princeton Applied Research, USA) incorporating a rotation disk electrode (RDE). A three-electrode cell, consisting of a glassy carbon electrode (GCE, as working electrode), a platinum (Pt) counterelectrode, and a Ag/AgCl reference electrode, was used for the measurement. The working electrode was covered with the part of a Ag-activated sample after being polished and cleaned by sonication. N_2 adsorption isotherms of the CFs were measured using a porosimeter (ASAP 2010, Micromeritics Ins. Corp., USA) at −196 °C with a relative pressure ranging from 10^{-6} to 1. The pore size distribution was determined using the Barrett, Joyner, and Halenda (BJH) method [40]. All experiments and measurements were performed four times and following data described with averaged values.

3. Results and discussion

Fig. 2a shows the size distribution of the spark-generated Ag aerosol nanoparticles, which was obtained using the SMPS system. The geometric mean electrical equivalent mobility diameter and geometric standard deviation were 10.1 nm and 1.37, respectively. The overall number and area concentrations were 1.14×10^6 particles/cm^3 and 4.58×10^8 nm^2/cm^3, respectively. Fig. 2a also shows the fractional (grade) collection efficiency of the CFs as a function of the particle size, which was calculated using the equation

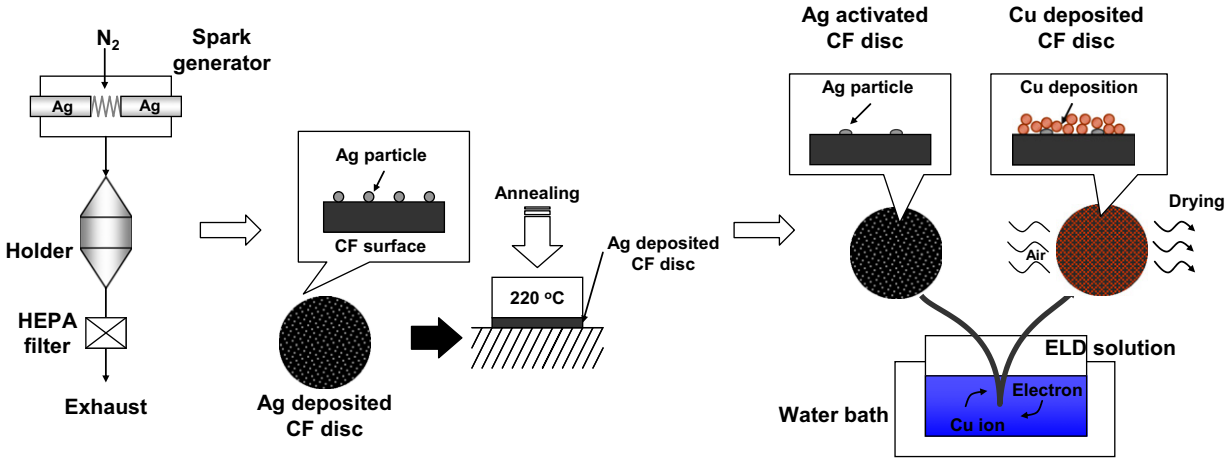

Fig. 1. Schematic of aerosol activation and subsequent ELD.

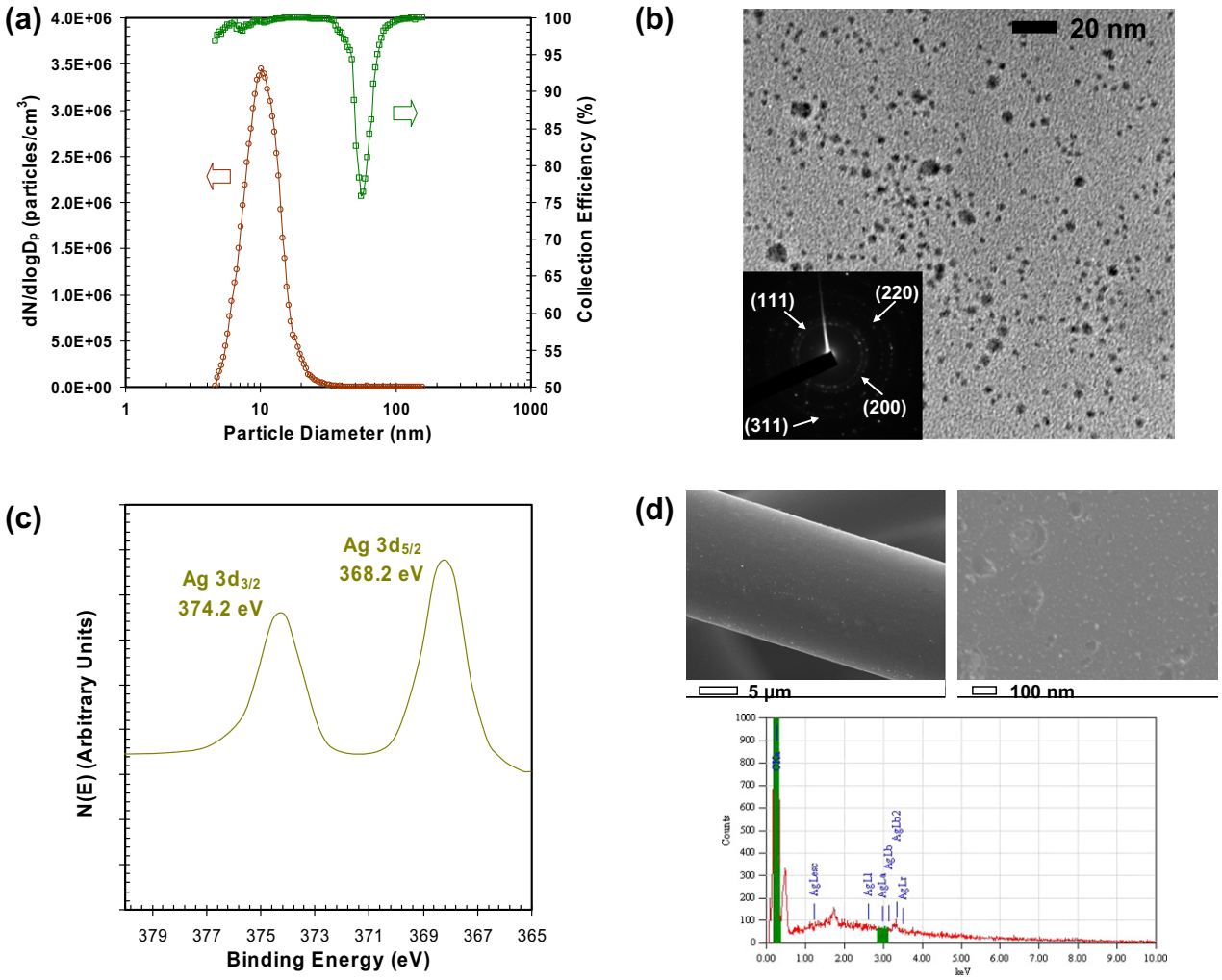

Fig. 2. Characterizations of aerosol activation: (a) particle size distribution of spark-generated aerosol nanoparticles and collection efficiency of CFs, (b) TEM micrograph and electron diffraction pattern of the nanoparticles, (c) XPS profile of the nanoparticles and (d) SEM micrographs (low and high magnitude) and EDX spectrum of aerosol-activated CFs.

$$\eta(D_p) = 1 - \left[\frac{C_f(D_p)}{C_i(D_p)}\right], \tag{1}$$

where $C_i(D_p)$ is the free-stream particle concentration and $C_f(D_p)$ is the concentration after filtration by the CFs. The overall collection efficiency is defined as follows:

$$\eta_{\text{overall}} = \frac{\int_0^\infty \eta(D_p) C_i(D_p) dD_p}{\int_0^\infty C_i(D_p) dD_p}. \tag{2}$$

The data shown in Fig. 2a resulted in η_{overall} = 98.2%, and indicated that a loss proportion of spark-generated Ag aerosol nanoparticles was about 2% in number count. The HRTEM micrograph (Fig. 2b) shows that sizes of the spark-generated nanoparticles were distributed around ~10 nm in mode diameter which was comparable to the particle size distribution in Fig. 2a. The electron diffraction pattern (inset of Fig. 2b) revealed the characteristic rings of a polycrystalline diffraction pattern. Spacing was observed at 2.36, 2.04, 1.44, and 1.22 Å, which were all within 2% of the value reported for the (1 1 1), (2 0 0), (2 2 0), and (3 1 1) face-centered cubic (fcc) Ag reflection (joint committee on powder diffraction standards (JCPDS) No. 1-1167), respectively. Fig. 2c shows the XPS profile corresponding to the Ag 3d spectrum region of the nanoparticles. Two peaks, observed at binding energies of 368.2 and 374.2 eV, corresponding to the Ag $3d_{3/2}$ and Ag $3d_{5/2}$ spectrum regions, respectively, were assigned to the Ag^0. Fig. 2d shows FESEM micrographs of a surface of the activated CFs with low (left) and high (right) magnitudes. Even though the left image had an indistinctly spotted surface, a number of spots (~10 nm in mode diameter) could be clearly observed in the right image. EDX results (also shown in Fig. 2d) showed a small amount of Ag (1.1 ± 0.25 wt.%) in the activated CF with carbon (C, 97.9 ± 3.10 wt.%) and oxygen (O, 1.0 ± 0.11 wt.%), which might have originated from the CF itself, was also detected. From the above results, a mass concentration (10.8 ± 0.55 μg/m^3 for overall) of Ag nanoparticles can be estimated and thus the activation intensity (I_a) is defined as [28]

$$I_a = Q \cdot t_a \cdot m_{\text{CF}}^{-1} \int_0^\infty \eta(D_p) C_m(D_p) dD_p, \tag{3}$$

where Q is the flow rate of N_2 gas, t_a is the activation time, m_{CF} is the mass of CFs disk, and $C_m(D_p)$ is the mass concentration of Ag nanoparticles. The activation intensity was approximately 48.4 μg Ag/g CF.

Fig. 3a shows FESEM micrographs on the CF surface after 30, 60, and 90 min immersion in Cu ELD solution. Initially, isolated nodular particles were observed after 30 min of deposition. The size of these nodules increased and coalescence of the nodules occurred after 60 min of deposition. However, for 60 min of deposition, the coverage was not complete; some voids were seen on the CFs

surface. When deposition time increased to 90 min, an electroless particle film (full surface coverage) could be clearly observed under FESEM. The improvement was due to the growth and coalescence of the particles in between the catalyst (Ag) seeds (i.e., Cu was deposited initially onto Ag seeds and then grew), forming a more uniform particle film [33]. Another micrograph of the 90 min deposition shows a thickness of the particle film. The sample preparation to measure easily the film thickness was performed under ultrasonic irradiation during DI water rinsing after Cu ELD. The ultrasonic irradiation induced a crack in the well-organized Cu film due to an intensive physical vibration within the film. The thickness of the film was about 460 ± 33.2 nm (the estimated lateral growth rate was about 5.1 nm/min), which did not show a definite void within the film. Separately, effects of the size and amount of catalyst seeds on ELD were introduced in [41] with a size control strategy of Ag seed particles in the aerosol state. The first image in Fig. 3b shows a different scaled micrograph of the Cu-deposited CFs for 60 min of deposition. The following three images show the EDX maps of the dotted area in the first image. These maps corresponded to C, Ag, and Cu, respectively. The dots in these images indicated the positions of each element in the first image. For example, Cu was concentrated in the area corresponding to the white fine spots in the first image, which shows that the spots on CFs were Cu (36.7 ± 4.60 wt.%). The following spectrum shows that the peaks situated at 0.93, 8.06, and 8.94 keV corresponded to the binding energies of Cu Lα, Cu Kα, and Cu Kβ, respectively. In addition, also shown are the binding energies of 2.98, 3.18, and 3.40 keV belonging to Ag Lα1, Ag Lβ1, and Ag Lβ2.15, respectively, which were derived from the catalytic activation. From the EDX compositions (table in Fig. 3b), it was found that the activated CFs contained C (62.7 ± 3.35 wt.%) and O (0.3 ± 0.04 wt.%), which might have originated from the CFs, while a small amount of Ag (0.3 wt.%) was also present. The mass deposition rates of Cu were obtained from the ICPAES analyses, and the rates for 30, 60, and 90 min of deposition were 0.25 ± 0.04, 0.81 ± 0.11, and 1.14 ± 0.09 mg Cu/g CF-min, respectively (table in Fig. 3b). Fig. 3c shows sharp peaks at around $2\theta = 43.4°$, 49.6°, and 74.2°. A comparison of these peaks with the data from JCPDS file (No. 4-0836) revealed that these peaks corresponded to the (1 1 1), (2 0 0), and (2 2 0) planes of the fcc phase of Cu. A preferred crystal orientation of (1 1 1) for the samples that have undergone a more than 60 min deposition was evidenced by the XRD results as shown in Fig. 3c. However, for a deposition time of less than 60 min, randomly oriented Cu grains were obtained. For a randomly oriented Cu sample, the $I_{(111)}/I_{(200)}$ intensity ratio was 1.88 ± 0.18. This factor increased to 3.15 ± 0.29 as deposition time increased to 60 min. Beyond 60 min of deposition, the $I_{(111)}/I_{(200)}$ ratio maintained a result of around 3.00 ± 0.30. It was noted that 60 min was the critical time that a continuously dense Cu film starts forming. This work shows that before a dense film was formed, the orientation of Cu grains was probably either random or preferred (1 0 0) [42], and the diffraction intensity on films below 30 min was too low to reach a solid conclusion. However, it was evident that once a dense film is formed, the (1 1 1) texture was quickly established. The average

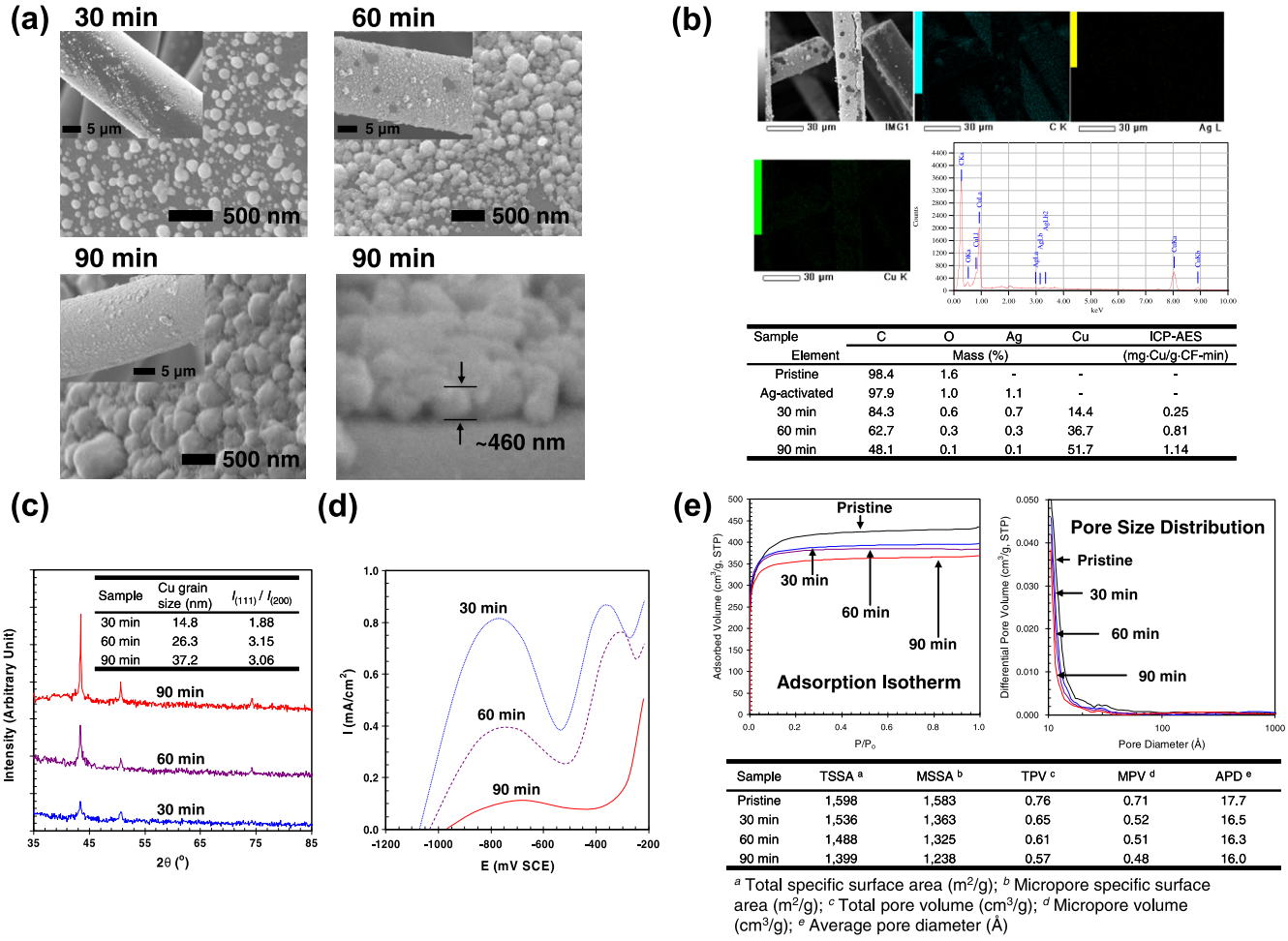

Fig. 3. Characterizations of ELD: (a) SEM micrographs as a function of ELD time, (b) EDX map results with chemical compositions, (c) XRD patterns of copper-deposited CFs, (d) current–potential curves for oxidation of glyoxylic acid during ELD and (e) adsorption isotherms, pore size distributions, and textural properties of CFs.

grain sizes estimated from the XRD line broadening of the (1 1 1) peak, according to Scherrer's equation ($t = 0.9\ \lambda/(B\cos\theta)$), were 14.8 ± 2.10, 26.3 ± 3.35, and 37.2 ± 5.41 nm for the depositions of 30, 60, and 90 min of deposition, respectively. From the estimations, the uniform Cu film (90 min ELD in Fig. 3a) consisted mainly of Cu grains with a size of about 40 nm in a dense manner. LSV was used to investigate the catalytic activity of the Ag nanoparticles for the oxidation of glyoxylic acid. Fig. 3d shows the LSV for glyoxylic acid oxidation on the activated CFs surface after 30, 60, and 90 min of deposition. The scan rate was 10 mV/s toward positive potentials from the open-circuit potential (OCP) to −250 mV. The Cu deposit after 30 min of deposition had an OCP of −1072 mV and two anodic peaks were observed. The first peak was at −764 mV and attributed to the oxidation of glyoxylic acid on the activated CFs surface still exposed to the electrolyte. The anodic peak current density for 60 min of deposition was significantly smaller than that of 30 min. It took a longer time for 90 min of deposition to reach its steady OCP of −971 mV. The anodic current density for the oxidation glyoxylic acid was very small, showing that the catalytic activity of the 90 min deposition for the oxidation of glyoxylic acid had nearly disappeared [34]. The shift in the OCP during Cu deposition in the electrolyte indicated that the Ag nanoparticles on the CF surface played an important role in the initial catalytic oxidation of glyoxylic acid in the deposition. Fig. 3e shows that a major uptake occurred at a relatively low pressure ($P/P_o < 1$) and a plateau was attained at $P/P_o \approx 0.3$, implying that all the CFs had microporous characteristics (type I isotherm) according to the IUPAC classification [43]. The specific surface area of the pristine CFs was the largest; however, it decreased as the amount of deposited Cu increased since the deposited Cu particles could block or occupy some pores of the pristine CFs. Even though a generation of surface area from the Cu deposition (i.e., Cu particle surface and void between Cu particles) might occur simultaneously, the area was remarkably smaller (<20 m^2/g) than the surface area of CFs (∼1600 m^2/g) and pore size mainly ranged over microporosity, so the area generation from the deposition did not affect the decrease of microporosity. Fig. 3e also shows that the pore size distributions of all the CFs were concentrated at pore diameters smaller than 20 Å. The table in Fig. 3e shows changes of the total surface area and total volume and changes in micropores, and in the average pore diameter, with increasing deposition time. However, the inherent microporous feature of CFs (volume of micropores ≫ volumes of meso- and macropores and average pore diameter <20 Å) [43] was retained, regardless of deposition time.

4. Conclusions

A novel ELD of Cu on CFs with environmentally friendly processes, Ag aerosol activation and subsequent nonformaldehyde Cu ELD, was developed. Spark-generated Ag aerosol nanoparticles (∼10 nm in mode diameter) were deposited (48.4 μg Ag/g CF in activation intensity) onto the surfaces of CFs. After annealing (at 220 °C in nitrogen atmosphere), the catalytically activated CFs were placed into solution for Cu deposition (at 82 °C). Homogeneous Cu coating (∼5.1 nm/min) on CFs was achieved until 90 min of deposition and the corresponding mass deposition rates and Cu grain sizes for 30–90 min of deposition were in the range of 0.25–1.14 mg Cu/g CF-min and 14.8–37.2 nm, respectively. The porosity of CFs decreased by depositing the Cu for 30–90 min, and the specific surface area and pore volume of CFs decreased from 1536 to 1399 m^2/g and from 0.65 to 0.57 cm^3/g, respectively. Our ELD for coating Cu may be attractive for various scientific and/or engineering applications because the catalytic activation of the CFs is simple, inexpensive, and environmentally friendly, and the nonformaldehyde Cu ELD is also attractive because of its relative environmental safety. A further study to verify the quality of the Cu film relating to activation intensities and bath chemicals for subsequent ELD with and without ultrasonic irradiation is now in preparation to publish elsewhere.

References

[1] J.H. Byeon, J.H. Park, K.Y. Yoon, J. Hwang, Langmuir 24 (2008) 5949–5954.
[2] Y.S. Huang, X.T. Zeng, I. Annergren, F.M. Liu, Surf. Coat. Technol. 167 (2003) 207–211.
[3] H. Du, S.W. Lee, J. Gong, C. Sun, L.S. Wen, Mater. Lett. 58 (2004) 1117–1120.
[4] X. Zhao, K. Hirogaki, I. Tabata, S. Okubayashi, T. Hori, Surf. Coat. Technol. 201 (2006) 628–636.
[5] J.H. Byeon, H.S. Yoon, K.Y. Yoon, S.K. Ryu, J. Hwang, Surf. Coat. Technol. 202 (2008) 3571–3578.
[6] B. Guo, S. Zhao, G. Han, L. Zhang, Electrochim. Acta 53 (2008) 5174–5179.
[7] J. Tong, L. Su, K. Haraya, H. Suda, J. Membr. Sci. 310 (2008) 93–101.
[8] E. Gasana, P. Westbroek, J. Hakuzimana, K.D. Clerck, G. Priniotakis, P. Kiekens, D. Tseles, Surf. Coat. Technol. 201 (2006) 3547–3551.
[9] S.-T. Shiue, C.-H. Yang, R.-S. Chu, T.-J. Yang, Thin Solid Films 485 (2005) 169–175.
[10] C.-Y. Huang, W.-W. Mo, M.-L. Roan, Surf. Coat. Technol. 184 (2004) 163–169.
[11] J. Jang, S.K. Ryu, J. Mater. Process Technol. 180 (2006) 66–73.
[12] H. Zhang, Y. Liu, J. Alloy. Compd. 458 (2008) 588–594.
[13] Y. Fan, H. Yang, X. Liu, H. Zhu, G. Zou, J. Alloy. Compd. 461 (2008) 490–494.
[14] Y.-Q. Kang, M.-S. Cao, X.-L. Shi, Z.-L. Hou, Surf. Coat. Technol. 201 (2007) 7201–7206.
[15] K.Y. Yoon, J.H. Byeon, C.W. Park, J. Hwang, Environ. Sci. Technol. 42 (2008) 1251–1255.
[16] C. Fukuhara, Y. Kamata, A. Igarashi, Appl. Catal. A 296 (2005) 100–107.
[17] S.J. Park, B.J. Kim, J. Colloid. Interface Sci. 282 (2005) 124–127.
[18] T. Homma, I. Komatsu, A. Tamaki, H. Nakai, T. Osaka, Electrochim. Acta 47 (2001) 47–53.
[19] H. Dai, H. Li, F. Wang, Surf. Coat. Technol. 201 (2006) 2859–2866.
[20] A. Vaškelis, A. Jagminienė, L. Tamašauskaitė-Tamašiūnaitė, R. Juškėnas, Electrochim. Acta 50 (2005) 4586–4591.
[21] Z.-C. Liu, Q.-G. He, P. Hou, P.-F. Xiao, N.-Y. He, Z.-H. Lu, Colloid Surf. A 257–258 (2005) 283–286.
[22] E. Touchais-Papet, M. Charbonnier, M. Romand, Appl. Surf. Sci. 138–139 (1999) 557–562.
[23] M. Šimor, J. Ráhel, M. Černák, Y. Imahori, M. Štefečka, M. Kando, Surf. Coat. Technol. 172 (2003) 1–6.
[24] D. Chen, Q. Lu, Y. Zhao, Appl. Surf. Sci. 253 (2006) 1573–1580.
[25] H. Esrom, Appl. Surf. Sci. 168 (2000) 1–4.
[26] S. Kreitz, C. Penache, M. Thomas, C.P. Klages, Surf. Coat. Technol. 200 (2005) 676–679.
[27] R.A. Weller, W.T. Ryle, A.T. Newton, M.D. McMahon, T.M. Miller, R.H. Magruder III, IEEE Trans. Nanotechnol. 2 (2003) 154–157.
[28] J.H. Byeon, B.J. Ko, J. Hwang, J. Phys. Chem. C 112 (2008) 3627–3632.
[29] J.E. Gray, P.R. Norton, K. Griffiths, Thin Solid Films 484 (2005) 196–207.
[30] S. Shulka, S. Seal, Z. Rahaman, K. Scammon, Mater. Lett. 57 (2002) 151–156.
[31] C.-Y. Kao, K.-S. Chou, Electrochem. Solid-State Lett. 10 (2007) D32–D34.
[32] J.B. Liu, W. Dong, P. Zhan, S.Z. Wang, J.H. Zhang, Z.L. Wang, Langmuir 21 (2005) 1683–1686.
[33] Y.Y. Shacham-Diamand, Electrochem. Solid-State Lett. 3 (2000) 279–282.
[34] J. Li, P.A. Kohl, J. Electrochem. Soc. 150 (2003) C558–C562.
[35] J. Li, H. Hayden, P.A. Kohl, Electrochim. Acta 49 (2004) 1789–1795.
[36] C. Subrahmanyam, D.A. Bulushev, L. Kiwi-Minsker, Appl. Catal. B 61 (2005) 98–106.
[37] Y. Matatov-Meytal, Y. Shindler, M. Sheintuch, Appl. Catal. B 45 (2003) 127–134.
[38] T.-H. Ko, K.-H. Hung, S.-S. Tzeng, J.-W. Shen, C.-H. Hung, Phys. Scr. T129 (2007) 80–84.
[39] J.H. Byeon, J.H. Park, J. Hwang, J. Aerosol. Sci. 39 (2008) 888–896.
[40] E.P. Barrett, L.G. Joyner, P.P. Halenda, J. Am. Chem. Soc. 73 (1951) 373–380.
[41] J.H. Byeon, J.-W. Kim, Langmuir, doi:10.1021/la101241x.
[42] Y.C. Ee, Z. Chen, L. Chan, A.K.H. See, S.B. Law, K.C. Tee, K.Y. Zeng, L. Shen, Thin Solid Films 462–463 (2004) 197–201.
[43] S. Brunauer, P.H. Emmett, E. Teller, J. Am. Chem. Soc. 60 (1938) 309–319.